


Molecular beam epitaxy of $\text{Sr}_5\text{Au}_2\text{O}_8$ thin filmsYoshiharu Krockenberger, Ai Ikeda, Hideki Yamamoto[✉], and Hiroo Omi*

NTT Basic Research Laboratories, NTT Corporation, 3-1 Morinosato-Wakamiya, Atsugi, Kanagawa 243-0198, Japan

 (Received 15 July 2020; revised 21 September 2021; accepted 6 December 2021; published 10 January 2022)

The synthesis of complex transition metal oxides using molecular beam epitaxy is well established with the exception of gold. Overcoming the oxophobicity of gold is a mandatory step towards an entire new section of complex transition metal oxides. Here, we show that $\text{Sr}_5\text{Au}_2\text{O}_8$ thin films can be epitaxially grown onto SrTiO_3 substrates using a high-efficiency radio-frequency-operated atomic oxygen source as an oxidizing agent. Stoichiometric atomic beam fluxes of strontium and gold were controlled by electron-impact emission spectroscopy. $\text{Sr}_5\text{Au}_2\text{O}_8$ thin films were grown at temperatures between 627 and 653 °C. Owing to the sensitivity of $\text{Sr}_5\text{Au}_2\text{O}_8$ thin films to environmental agents, e.g., water and CO_2 , we capped them with a 300-nm layer of Se or a 200-nm layer of Au.

DOI: [10.1103/PhysRevMaterials.6.013401](https://doi.org/10.1103/PhysRevMaterials.6.013401)

I. INTRODUCTION

Oxide materials, particularly complex transition metal oxide materials, are perceptibly distinct from other materials systems as they allow for crystal symmetries where inherent electronic correlations may thrive. For $3d$ complex transition metal oxides, quantum states, e.g., superconductivity in cuprates or ferromagnetism in manganites, are well known. The techniques of single-crystal synthesis methods have allowed scientists to gain invaluable in-depth understanding of those quantum phenomena. However, with these synthesis methods, superlattices are not accessible, and other means are required to overcome such materials synthesis limitations. Thin-film synthesis methods, e.g., molecular beam epitaxy (MBE) or pulsed laser deposition, are synthesis methods that allow one to combine unequal complex transition metal oxides with atomically resolved precision. Nonetheless, in-depth knowledge of the synthesis parameter space of each constituent complex transition metal oxide is required to design novel materials. Crystal synthesis limitations are fundamental and go well beyond $3d$ complex transition metal oxides. For example, Sr_2RuO_4 [1] and Nd_2PdO_4 [2,3] are $4d$ complex transition metal oxides where pulsed laser deposition or molecular beam epitaxy are instrumental for the development of single-crystalline thin films and combinations between them. Certainly, this is also true for $5d$ complex transition metal oxides, e.g., iridates [4] or osmates [5]. For complex gold oxides (aurates), little is known and even less so when it comes to aurate thin films. This is not surprising as gold is known to be inert against almost any chemical reaction. Formally, two valence states of gold are known [6], Au^+ and Au^{3+} . While the monovalent state of gold is found in electrophilic compounds, e.g., gold-chloroquine [7], the common state is Au^{3+} . Simple aurates, e.g., Au_2O_3 , are ther-

modynamically unstable at ambient conditions due to their negative Gibbs free energy [6,8–11]. The d^8 character of Au^{3+} imposes constraints as to what coordinations are possible. In cuprates, edge-sharing and corner-sharing CuO_2 plaquettes are known, for example, in Li_2CuO_2 (and KCuO_2) and Sr_2CuO_3 (and $\text{Sr}_{14}\text{Cu}_{24}\text{O}_{41}$), respectively [12,13]. While the coordination of Cu^{2+} takes on three different modifications in oxides, gold Au^{3+} prefers a square or distorted square-planar coordination [14]. It is for this reason that AuO_4 polygons are formed among the many aurates known thus far [15]. Notably, LaAuO_3 [16] has been known for a long time, and the incorporation of a rare earth element into the La_2O_3 - Au_2O_3 system supports the thermodynamic stability [17] of the gold-oxide state; this has been verified also for $\text{La}_4\text{Au}_2\text{O}_9$ [18], a rare-earth aurate of even higher complexity. Adding an additional alkaline element to the La_2O_3 - Au_2O_3 thermodynamic system, in fact, greatly enhances the thermodynamic stability of the Au^{3+} state, and it becomes comparable to perovskite materials containing $3d$ elements. Single-crystal analysis of $\text{La}_2\text{Li}_{1/2}\text{Au}_{1/2}\text{O}_4$ [19] and, later on, neutron diffraction experiments [20,21] have shown that isolated AuO_4 plaquettes are stabilized and that they are separated by LiO_4 plaquettes [22]. Moreover, CaAu_2O_4 [23,24], SrAu_2O_4 , and BaAu_2O_4 [25] are alkaline-earth aurates that also show isolated AuO_4 plaquettes. These plaquettes are also found in more complex aurates, e.g., $\text{Sr}_5\text{Au}_2\text{O}_8$ [26] as well as $\text{Ba}_9\text{Au}_2\text{O}_{12}$ [27].

Superconductivity, an electronic state known from some complex transition metal oxides with high-symmetry features, i.e., planes, is a worthwhile motivator being looked for. However, the synthesis of such complex transition metal oxides is not a one-way street; one is confronted with many obstacles, and it seems that those obstacles are overwhelming for aurates. Details of the reaction between Au and O_2 have been analyzed [28], and it was found that molecular oxygen does not oxidize gold [10]. This is not surprising, and other means have to be taken to oxidize gold, which are commonly hydrothermal methods in combination with strong oxidizing agents such as KClO_4 . As the goal of this study is to

*Present address: Yamato University, Katayama-cho, Osaka 564-0082, Japan.

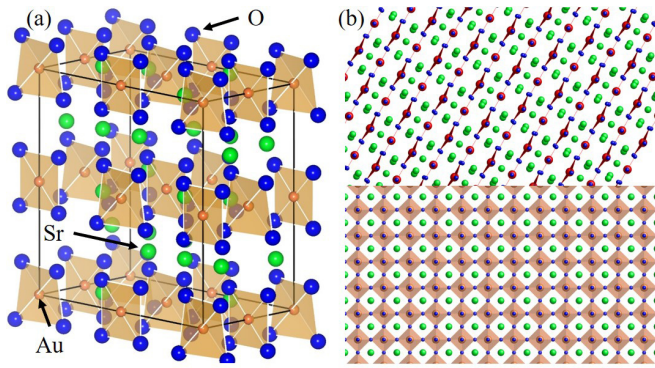


FIG. 1. In (a), the perspective presentation of the crystal structure of $\text{Sr}_5\text{Au}_2\text{O}_8$ is shown with the Au^{3+} ions coordinated by four O^{2-} ions in a square plaquette. In (b), the epitaxial arrangement between $\text{Sr}_5\text{Au}_2\text{O}_8$ and SrTiO_3 is shown. Here, (111) $\text{Sr}_5\text{Au}_2\text{O}_8$ is parallel to the (001) SrTiO_3 plane.

synthesize an aurate containing AuO_4 plaquettes by molecular beam epitaxy, an oxidizing agent, sufficient to oxidize gold under ultrahigh vacuum, should be considered.

II. SYNTHESIS AND RESULTS

The space group of $\text{Sr}_5\text{Au}_2\text{O}_8$ is orthorhombic ($D_2^7 - F_{222}$, space group 22), and the orthorhombicity is small, i.e., the Wyckoff position parameters of oxygen are rather close to high-symmetry positions [29]. In detail, the a - and b -axis lattice constants are less than 0.4 pm apart, and we therefore consider the crystal symmetry to be tetragonal. While such a simplification is certainly useful for the further considerations of an epitaxial growth process, common perovskite-type substrate materials, e.g., SrTiO_3 ($a = 3.905 \text{ \AA}$), have lattice constants that are, at first sight, somewhat compatible with the in-plane lattice constant of $\text{Sr}_5\text{Au}_2\text{O}_8$ ($a = 11.74 \text{ \AA}$). In other words, a 3×3 patch of SrTiO_3 unit cells appears to stabilize a single unit cell of $\text{Sr}_5\text{Au}_2\text{O}_8$. Such geometric considerations might be reasonable if the crystal structure of $\text{Sr}_5\text{Au}_2\text{O}_8$ (Fig. 1) would be a perovskite-related structure. It is therefore highly unlikely that c -axis-oriented $\text{Sr}_5\text{Au}_2\text{O}_8$ would be stabilized on (001) SrTiO_3 substrates. An alternative geometric arrangement might be that the (111) plane of $\text{Sr}_5\text{Au}_2\text{O}_8$ is parallel to the (001) plane of the SrTiO_3 substrate. At the beginning of this investigation into the growth of complex aurates by molecular beam epitaxy we did not try to rule out any possible outcome, and we therefore scanned the synthesis parameters of $\text{Sr}_5\text{Au}_2\text{O}_8$ thin films for the following substrate materials: (001) SrTiO_3 , (110) SrTiO_3 , (110) YAlO_3 , (001) KTaO_3 , (001) $(\text{LaAlO}_3)_{0.3}(\text{Sr}_2\text{AlTaO}_6)_{0.7}$ (LSAT), (001) MgO , (0001) Al_2O_3 , $(1\bar{1}02)$ Al_2O_3 , (100) and (001) SrLaAlO_4 , (110) RScO_3 ($R = \text{Tb, Dy, Gd, Sm, Nd}$), (001) ZrO_2 , (001) MgAl_2O_4 , (001) SrLaGaO_4 , (110) NdAlO_3 , and (110) NdGaO_3 substrates. In addition to these oxide substrates, we also used alkaline-earth halide substrates, i.e., (001) CaF_2 and BaF_2 . A highly efficient atomic oxygen source (Fig. 2) that allows for *in situ* production of oxygen atoms at low radio-frequency (rf) power, is exigent to readily oxidize gold [30] as oxygen molecules cannot surmount the reaction kinetic barrier of gold [10,31,32]. Very little is known as

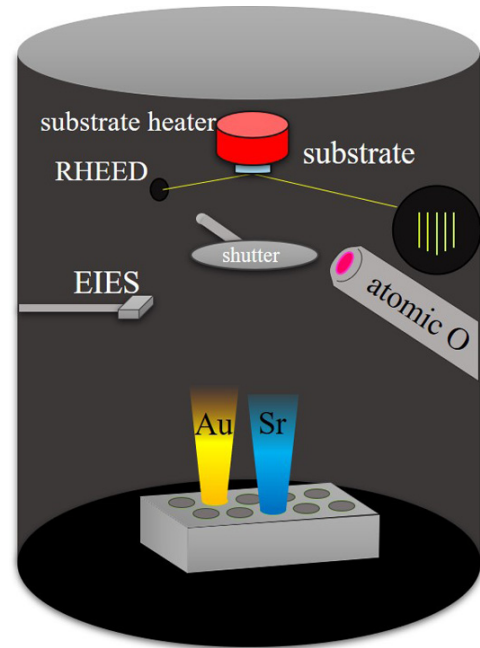


FIG. 2. Sketch of the molecular beam epitaxy system used for the synthesis of $\text{Sr}_5\text{Au}_2\text{O}_8$ thin films. Au and Sr are being evaporated using Thermionics electron guns in a custom-designed vacuum chamber with a base pressure $< 10^{-9}$ Torr. The stoichiometries of the fluxes of Au and Sr are controlled using an electron impact emission spectroscopy (EIES) technique. A custom-designed high-efficiency radio-frequency-powered atomic oxygen source is used as an oxygen source. The substrate temperature of SrTiO_3 substrates is controlled using a closed-loop pyrometer system. The growth is monitored using reflection high-energy electron diffraction (RHEED).

to the thermodynamic boundary conditions of aurates, and this is particularly the case for aurate thin films. As a first step we looked at the thermodynamic boundary conditions of the $4 \text{ Au} + 3 \text{ O}_2 \rightleftharpoons 2 \text{ Au}_2\text{O}_3$ (Fig. 3) with data taken from Refs. [33–35]. According to an earlier report on the growth of Au_2O_3 single crystals [9], synthesis temperatures of $270 \text{ }^\circ\text{C}$ and an oxygen equilibrium pressure of 300 atm using hydrothermal conditions resulted in a single-crystal growth rate of $\sim 400 \text{ nm/h}$. Such a growth rate is insignificantly different from typical growth rates in molecular beam epitaxy, and we tried to mimic these conditions by keeping the growth temperature constant at $270 \text{ }^\circ\text{C}$ and varying the flow rate of oxygen through a high-efficiency custom-designed rf atomic oxygen source [2,36] operated at 300 W between 0.2 and 8.0 SCCM (SCCM denotes cubic centimeter per minute at STP) in intervals of 0.2 SCCM. Sr and Au were evaporated from metal sources using Thermionics electron guns, and the individual flux rates were controlled by real-time electron impact emission spectroscopy (EIES). Throughout the experiments presented here we maintained an atomic flux ratio of Sr and Au that corresponds to a stoichiometry of $\text{Sr}:\text{Au} = 5:2$. As a result, we found that the films grown on any of the substrate materials listed above are polycrystalline gold with a common orientation of (111) Au parallel to the substrate surface. Also, the existence of polycrystalline Au was independently confirmed from resistivity measurements which

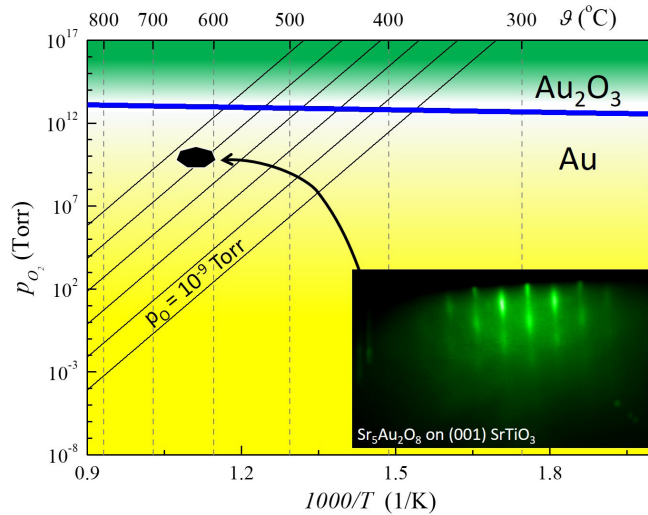


FIG. 3. Thermodynamic phase diagram of Au_2O_3 with data taken from Peuckert [33] (blue line). The presence of Sr and/or Nd may enhance the thermodynamic stability with respect to Au_2O_3 . The marked area represents the conditions used for growth of single-phase thin films of $\text{Sr}_5\text{Au}_2\text{O}_8$ by molecular beam epitaxy. Equilibrium lines for $2\text{O} \rightleftharpoons \text{O}_2$ (atomic oxygen) are shown as well. The thermodynamic area used for the synthesis of $\text{Sr}_5\text{Au}_2\text{O}_8$ thin films is nearly identical to conditions used for the bulk synthesis by Weinreich and Müller-Buschbaum [26]. The inset shows a RHEED image taken after 8 min of growth and during the deposition process of $\text{Sr}_5\text{Au}_2\text{O}_8$ along the $[\bar{1}02]$ direction.

indicated metallic conduction. This is particularly remarkable as the films were cooled to room temperature while the atomic oxygen source remained on. From this result we drew two conclusions. First, the reaction kinetics between Au and O atoms might be sufficient to form isolated Au_2O_3 and SrO molecules though the reaction between them has been stymied under ultrahigh vacuum conditions. The subsequent characterization by x-ray diffraction is performed under ambient conditions. Owing to the negative Gibbs energy of Au_2O_3 , rapid decomposition gives rise to x-ray diffraction data indicating polycrystalline gold. As this is also true for Au_2O_3 single crystals, the volume of the thin films is several orders of magnitude smaller compared with the reported single crystals. Second, we suspect that the surface diffusion length of Au_2O_3 and SrO is too short at such a synthesis temperature and this further impedes long-range order. As the decomposition temperature of pure Au_2O_3 is about 350°C [37] and no long-range order has been observed even for Au_2O_3 films grown by Ne/ O_2 sputter processes [38], higher synthesis temperatures are suggested. On a side note, to make matters worse, the stability of Au_2O_3 is further reduced by common environmental agents, e.g., water or carbon dioxide [39]. Subsequently, we applied synthesis conditions at higher synthesis temperatures while maintaining the oxygen flow rate at 2.0 SCCM and the stoichiometry of Sr: Au = 5:2. For each growth temperature, we determined the crystalline quality of the resultant film using x-ray diffraction. For the experiments discussed here, we kept the growth time constant at 10 min, and this allowed us to quantitatively compare the observed x-ray diffraction intensities for films grown at different synthesis temperatures.

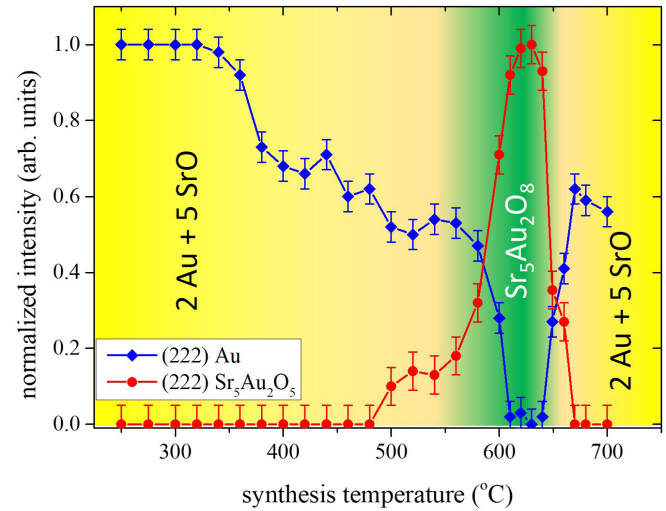


FIG. 4. Plot of the normalized x-ray diffraction intensities of (222) Au and (222) $\text{Sr}_5\text{Au}_2\text{O}_8$ as a function of the synthesis temperature. After the synthesis of each $\text{Sr}_5\text{Au}_2\text{O}_8$ film by molecular beam epitaxy, the samples were cooled to room temperature under flowing atomic oxygen of 2.0 SCCM. Thereafter, the samples were transferred under ultrahigh vacuum into a load-lock chamber and brought to atmospheric pressure by argon gas. Within a time window of less than 5 min after removal of the sample from the MBE loading chamber, x-ray diffraction measurements were started to be carried out. For the sake of time efficiency, the $\text{Sr}_5\text{Au}_2\text{O}_8$ used here was not capped by either selenium or gold. The plotted normalized intensities are therefore subject to an error of 10%. Note that samples that mainly show gold on the diffraction pattern are stable in air and the capping process protects only the volume fraction made up of $\text{Sr}_5\text{Au}_2\text{O}_8$. Here, the films were deposited on (001) SrTiO_3 substrates.

For synthesis temperatures of 250°C the x-ray diffraction intensity of the (222) diffraction peak of Au is highest, and we normalized the (222) Au diffraction intensities for all films to that value. In Fig. 4, we plot the normalized x-ray diffraction intensity of (222) Au as a function of the synthesis temperature. Similarly, we plot the normalized x-ray diffraction intensity of the (222) $\text{Sr}_5\text{Au}_2\text{O}_8$ phase in Fig. 4. Up to a synthesis temperature of 500°C , the phase volume of gold decreases monotonically while little can be seen from the designated phase. Increasing the synthesis temperature further up to 640°C significantly enhances the coherent volume of $\text{Sr}_5\text{Au}_2\text{O}_8$ while gold is now virtually absent. Attempts to measure the electric resistivity of such a sample failed owing to the resistivity limitations of our experimental setup of $\sim\text{k}\Omega\text{cm}$. In other words, these results suggest that gold has not accumulated in the film material but instead it has been incorporated into the crystal structure of $\text{Sr}_5\text{Au}_2\text{O}_8$. Note that at low growth temperatures, metallic gold films form with (111) growth orientation and thus the (111) Au planes are parallel to the substrate. In Fig. 5, the x-ray diffraction pattern of a $\text{Sr}_5\text{Au}_2\text{O}_8$ thin film grown on (001) SrTiO_3 is shown. For the moment, the film is single phase, and the growth direction is oriented along the [111] axis. Further increasing the synthesis temperature above 650°C resulted again in the formation of metallic gold films. Note that during this study we did not

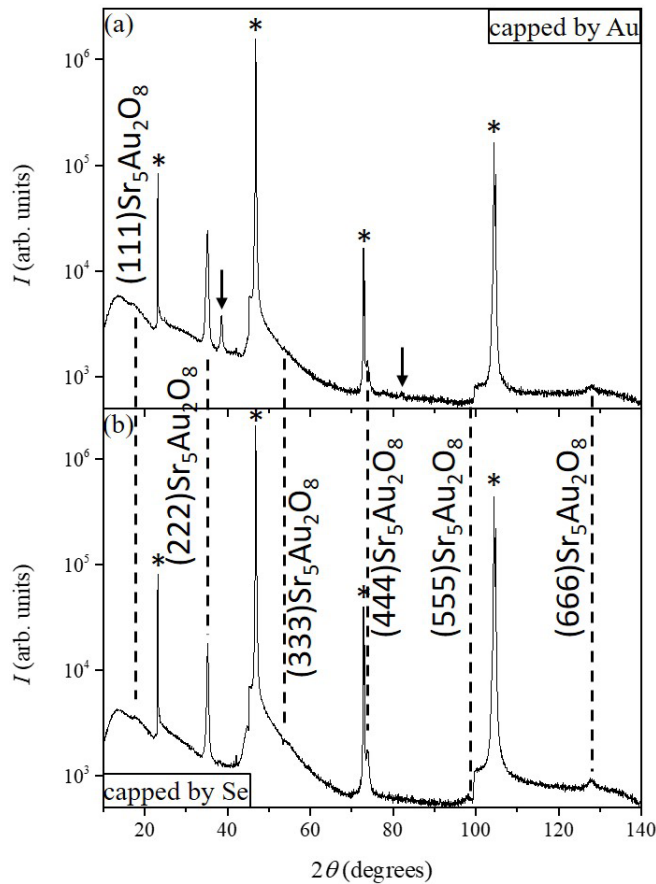


FIG. 5. X-ray diffraction patterns of monolithic $\text{Sr}_5\text{Au}_2\text{O}_8$ film grown onto (001) SrTiO_3 substrates. The $\text{Sr}_5\text{Au}_2\text{O}_8$ films are (111) oriented. To prevent exposure of the $\text{Sr}_5\text{Au}_2\text{O}_8$ film to water or CO_2 , the $\text{Sr}_5\text{Au}_2\text{O}_8$ film has been capped by a 200-nm Au layer (a) or a 300-nm Se layer (b). The additional diffraction peaks in (a) marked by arrows correspond to (111) and (222) Au diffraction peaks and stem from the capping layer. Note that for Se-capped $\text{Sr}_5\text{Au}_2\text{O}_8$ films, diffraction peaks associated with elemental Au are absent. X-ray diffraction peaks marked by an asterisk denote (00 l) SrTiO_3 peak positions.

observe the formation of other aurates, e.g., SrAu_2O_4 . For the following experiments, we fixed the synthesis temperature to $\sim 635^\circ\text{C}$ and varied the oxygen flow rate through the atomic oxygen source. Single-phase thin films of $\text{Sr}_5\text{Au}_2\text{O}_8$ were grown for oxygen flow rate in the range of 1.5–2.5 SCCM. Low oxygen flow rates were insufficient to oxidize gold as determined by RHEED. On the higher end of the oxygen flow range, flow rates as high as 4.0–8.0 SCCM also impeded the formation of gold oxides. For low oxygen flow rates, this can be attributed to a low oxidizing potential, whereas for high oxygen flow rates the associated increase in chamber pressure enhances the recombination rate of oxygen atoms prior to the formation of gold oxides. Note that the typical pressure in the MBE chamber is about 4×10^{-6} Torr at an oxygen flow rate of 2 SCCM.

During the course of our experiments we noticed a significant drop in x-ray diffraction intensity after leaving the sample in air for some time. In detail, on our Bruker D2 Phaser, it takes 16 min to record one x-ray diffraction spectrum while

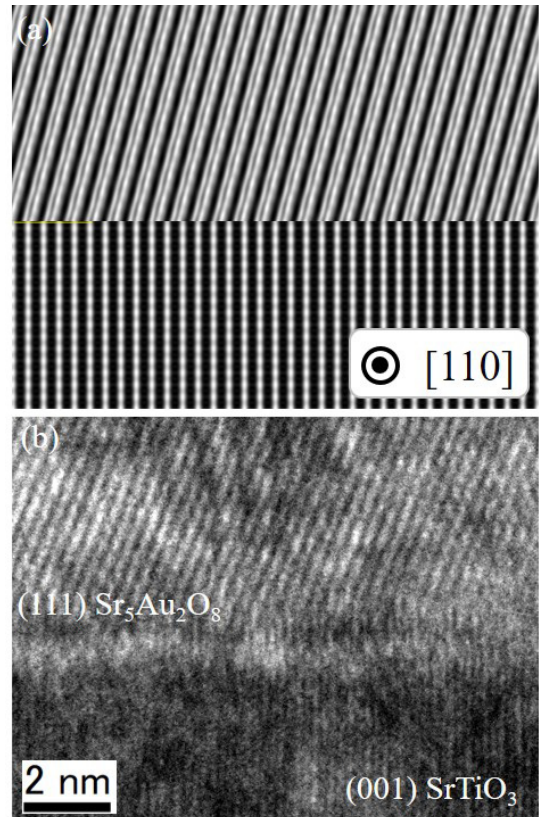


FIG. 6. (a) Simulation of the cross-sectional TEM image at the interface region between (111) $\text{Sr}_5\text{Au}_2\text{O}_8$ and (001) SrTiO_3 . For the simulation, the software package RECIPRO [41] was used. In (b), the cross-sectional, low-temperature TEM image of a $\text{Sr}_5\text{Au}_2\text{O}_8$ film grown on (001) SrTiO_3 substrates is shown. The (111) plane of the $\text{Sr}_5\text{Au}_2\text{O}_8$ film is parallel to the (001) plane of SrTiO_3 . The [110] axis of $\text{Sr}_5\text{Au}_2\text{O}_8$ is parallel to the [010] axis of SrTiO_3 . This TEM image was recorded at 77 K in order to minimize the thermal degradation brought by the measurement electron beam. The flow of liquid nitrogen in the sample stage gives rise to mechanical vibrations, and the TEM imagery therefore appears noisy.

scanning over $10 < 2\theta < 140^\circ$. An immediate rerun gives rise to a 30% drop in x-ray diffraction intensity if the measured phase was initially $\text{Sr}_5\text{Au}_2\text{O}_8$. Over the stretch of a 24-h period, the diffracted peaks vanished. The ambient conditions of the x-ray diffraction measurement are 24°C with a relative humidity level of 65%. We speculated that such conditions may not be appropriate and therefore capped the $\text{Sr}_5\text{Au}_2\text{O}_8$ thin films with 300 nm of Se using a custom-designed, copper-reinforced, temperature-controlled, water-chilled effusion cell operated at 216°C which corresponds to a vapor pressure of 5×10^{-3} Torr. Selenium capping is a common process to shield sensitive materials from environmental conditions [40]. After capping with selenium, the observed x-ray diffraction intensity remained constant even after 2 weeks and therefore independent of the timing of the measurement. Selenium is an insulating material, therefore causing the common charge-up problem of high-resolution transmission electron microscopy (TEM). To bypass this hitch for some films, a solid gold film with 200-nm thickness was deposited instead at 25°C . We confirmed by x-ray diffraction that after the deposition of

TABLE I. Substrate materials and associated substrate orientations used for the growth of $\text{Sr}_5\text{Au}_2\text{O}_8$ thin films.

Substrate material	Orientation	$\text{Sr}_5\text{Au}_2\text{O}_8$ growth
NdAlO ₃	(110)	no
NdGaO ₃	(110)	no
YAlO ₃	(001)	no
KTaO ₃	(001)	no
MgO	(001)	no
TbScO ₃	(110)	no
GdScO ₃	(110)	no
SmScO ₃	(110)	no
NdScO ₃	(110)	no
PrScO ₃	(110)	no
DyScO ₃	(110)	no
MgAl ₂ O ₄	(001)	no
Al ₂ O ₃	(0001)	no
Al ₂ O ₃	(1 $\bar{1}$ 02)	no
SrLaAlO ₄	(001)	no
SrLaAlO ₄	(100)	no
SrTiO ₃	(001)	yes
SrTiO ₃	(110)	no
SrLaGaO ₄	(001)	no
ZrO ₂	(001)	no
LSAT	(001)	no

gold, the underlying $\text{Sr}_5\text{Au}_2\text{O}_8$ film remained intact though the overall intensities, including the intensities of the substrate, were reduced by 22% (Fig. 5). Initial attempts to perform a cross-sectional TEM measurement, using focused ion-beam milling and a JEOL 200F electron microscope, failed. In detail, during the measurement, clear modifications could be made visible, and these alterations produced metallic gold dendrites. This behavior even persisted for the smallest measurement currents, and the recorded images were inconclusive. Absorption of the implanted heat by the measurement current seemed therefore unavoidable, and we deployed a low-temperature sample stage which was cooled by flowing liquid nitrogen. Eventually, we were able to resolve the atomic image of a $\text{Sr}_5\text{Au}_2\text{O}_8$ thin film epitaxially grown onto a (001) SrTiO_3 substrate by molecular beam epitaxy (Fig. 6). From Fig. 6, we can derive the following conclusions associated with the epitaxial relation of film and substrate. $\text{Sr}_5\text{Au}_2\text{O}_8$ thin films are indeed epitaxially grown, and their lattice parameters appear to maintain values known from bulk samples. However, there might be additional mechanisms that influence the growth of $\text{Sr}_5\text{Au}_2\text{O}_8$ thin films. In Table I, we compare substrate materials and their orientations used in this paper. Yet (001) SrTiO_3 substrate is the only choice that allowed us to confirm the formation of $\text{Sr}_5\text{Au}_2\text{O}_8$ thin films. In detail, while the substrate lattice mismatches of SrTiO_3 or LSAT are not that far apart (<1%), we could not confirm the formation of the $\text{Sr}_5\text{Au}_2\text{O}_8$ phase on LSAT substrates.

III. DISCUSSION

At the beginning of our investigation into the growth of aurates by molecular beam epitaxy it was unclear whether or not this was feasible. Also, the nature of the Au-O bond might give rise to rather unconventional epitaxial relations, and it is for this reason that the resulting orientation of the $\text{Sr}_5\text{Au}_2\text{O}_8$ thin film where the [111] axis is parallel to the [001] axis of SrTiO_3 is unexpected. At this point, domain mixing of (111) and (1 $\bar{1}$ 0) domains cannot be ruled out owing to the similarities of the lattice parameter lengths in *b* and *c* directions. The situation is further complicated by there being two different Au^{3+} sites in the unit cell, and therefore only every next-nearest AuO_4 plaquette is actually a plaquette. Au^{3+} ions located at *4a* sites are about 8 pm displaced out of the AuO_4 plaquettes and are therefore not aligned parallel. From the electron diffraction Laue pattern taken of a $\text{Sr}_5\text{Au}_2\text{O}_8$ film, we estimated the bond length of the gold-oxygen bond $d_{\text{Au-O}} \approx 2.02 \pm 0.05$ Å, which is significantly longer than what is seen for other complex transition metal oxides. However, if the unit cell of $\text{Sr}_5\text{Au}_2\text{O}_8$ is aligned along the [111] direction, the average distance $d_{\text{Au-Au}} = \frac{1}{3}a \approx 3.91$ Å, and this would allow each Au^{3+} ion to be at an identical position on a TiO_2 -terminated substrate. It is known that the two different crystallographic Au sites in $\text{Sr}_5\text{Au}_2\text{O}_8$ [26] have slightly different associated bond lengths of 2.00 and 2.02 Å, respectively. From the crystallographic analysis of our thin-film samples we cannot distinguish these two sites. Nonetheless, our average gold-oxygen bond lengths do not deviate more than 20 pm from the bulk values. The observed growth configuration here (Fig. 6) seems to confirm this scenario. Finally, the fact that aurates can be synthesized by molecular beam epitaxy within certain thermodynamic boundaries gives hope for novel material systems, particularly superlattices built in combination with other complex transition metal oxides. While the Au^{3+} state is the most stable configuration and a stable Au^{2+} ion was only recently observed [42], $\text{Sr}_5\text{Au}_2\text{O}_8$ thin films may open a way to investigate novel topological effects owing to the large spin-orbit coupling in complex aurates. As the electronic ground state of such aurates is $5d^8$, they are all intrinsically insulators with electronic band gap values in the range of 1.4 eV [43].

In conclusion, we have synthesized high-quality single-crystalline thin films of $\text{Sr}_5\text{Au}_2\text{O}_8$ on (001) SrTiO_3 substrates using molecular beam epitaxy in tandem with an atomic oxygen source. The $\text{Sr}_5\text{Au}_2\text{O}_8$ thin films are grown in a relaxed way, and further investigations are required in order to synthesize aurates that have infinitely connected AuO_2 planes [44] that may enable the induction of superconductivity.

ACKNOWLEDGMENTS

The authors acknowledge Takayuki Ikeda for support in STEM measurements. The authors acknowledge the support from K. Oguri and Y. Taniyasu. The authors also appreciate the support of Y. Tanaka in providing halide substrates.

[1] Y. Krockenberger, M. Uchida, K. S. Takahashi, M. Nakamura, M. Kawasaki, and Y. Tokura, Growth of superconducting Sr_2RuO_4 thin films, *Appl. Phys. Lett.* **97**, 082502 (2010).

[2] Y. Nanao, A. Ikeda, M. Naito, H. Yamamoto, K. Kumakura, and Y. Krockenberger, Molecular beam epitaxy of Nd_2PdO_4 thin films, *AIP Adv.* **7**, 075006 (2017).

- [3] Y. Nanao, Y. Krockenberger, A. Ikeda, Y. Taniyasu, M. Naito, and H. Yamamoto, Crystal growth and metal-insulator transition in two-dimensional layered rare-earth palladates, *Phys. Rev. Mater.* **2**, 085003 (2018).
- [4] J. S. Lee, Y. Krockenberger, K. S. Takahashi, M. Kawasaki, and Y. Tokura, Insulator-metal transition driven by change of doping and spin-orbit interaction in Sr_2IrO_4 , *Phys. Rev. B* **85**, 035101 (2012).
- [5] Y. Wakabayashi, Y. Krockenberger, N. Tsujimoto, T. Boykin, S. Tsuneyuki, and H. Yamamoto, Ferromagnetism above 1000 K in a highly cation-ordered double-perovskite insulator Sr_3OsO_6 , *Nat. Commun.* **10**, 535 (2019).
- [6] H. Shi, R. Asahi, and C. Stampfl, Properties of the gold oxides Au_2O_3 and Au_2O : First-principles investigation, *Phys. Rev. B* **75**, 205125 (2007).
- [7] M. Navarro, C. Hernández, F. Vásquez, H. Goitia, L. Ojeda, M. Velásquez, and G. Fraile, Syntheses, characterization, and biological evaluation of new zinc-and gold-chloroquine diphosphate complexes, *Transit. Met. Chem.* **33**, 893 (2008).
- [8] O. Knacke, O. Kubaschewski, and K. Hesselmann, *Thermochemical Properties of Inorganic Substances* (Springer-Verlag, Berlin, 1991), Vol. 1.
- [9] E. Schwarzmann, J. Mohn, and H. Rumpel, Notizen: Über Einkristalle von Goldoxid Au_2O_3 . / On single crystals of gold oxide Au_2O_3 , *Z. Naturforsch. B* **31**, 135 (1976).
- [10] H. Tsai, E. Hu, K. Perng, M. Chen, J. Wu, and Y. Chang, Instability of gold oxide Au_2O_3 , *Surf. Sci.* **537**, L447 (2003).
- [11] P. G. Jones, H. Rumpel, E. Schwarzmann, G. M. Sheldrick, and H. Paulus, Gold(III) oxide, *Acta Cryst. B* **35**, 1435 (1979).
- [12] N. Brese, M. O’Keeffe, R. Von Dreele, and V. Young, Crystal structures of NaCuO_2 and KCuO_2 by neutron diffraction, *J. Solid State Chem.* **83**, 1 (1989).
- [13] S. Drechsler and T. Mishonov, *High- T_c Superconductors and Related Materials: Material Science, Fundamental Properties, and Some Future Electronic Applications*, Nato Science Partnership Subseries Vol. 3 (Springer, Dordrecht, 2012).
- [14] D. Waroquiers, X. Gonze, G. Rignanese, C. Welker-Nieuwoudt, F. Rosowski, M. Göbel, S. Schenk, P. Degelmann, R. André, R. Glaum, and G. Hautier, Statistical analysis of coordination environments in oxides, *Chem. Mater.* **29**, 8346 (2017).
- [15] H. Müller-Buschbaum, Zur Kristallchemie der Oxoaurate, *Z. Anorg. Allg. Chem.* **628**, 2559 (2002).
- [16] M. Ralle and M. Jansen, Synthesis and crystal structure determination of LaAuO_3 , *J. Solid State Chem.* **105**, 378 (1993).
- [17] L. Ono and B. Roldan Cuenya, Formation and thermal stability of Au_2O_3 on gold nanoparticles: Size and support effects, *J. Phys. Chem. C* **112**, 4676 (2008).
- [18] M. Ralle and M. Jansen, Darstellung und Kristallstruktur des neuen Lanthanaurates $\text{La}_4\text{Au}_2\text{O}_9$, *J. Alloys Compd.* **203**, 7 (1994).
- [19] W. Pietzuch, S. A. Warda, W. Massa, and D. Reinen, Die Kristallstruktur von $\text{La}_2\text{Li}_{1/2}\text{Au}_{1/2}\text{O}_4$ und bindungschemische Aspekte, *Z. Anorg. Allg. Chem.* **626**, 113 (2000).
- [20] J. Kurzman, S. Moffitt, A. Llobet, and R. Seshadri, Neutron diffraction study of $\text{La}_4\text{LiAuO}_8$: Understanding Au^{3+} in an oxide environment, *J. Solid State Chem.* **184**, 1439 (2011).
- [21] T. Forbes, J. Kurzman, R. Seshadri, and A. Navrotsky, The energetics of $\text{La}_4\text{LiAuO}_8$, *J. Mater. Res.* **26**, 1188 (2011).
- [22] J. Delgado, V. García Rojas, and G. Gauthier, Synthesis and characterization of gold-containing oxides of K_2NiF_4 or Nd_2CuO_4 structure type, *Gold Bull.* **51**, 35 (2018).
- [23] L. Anja and R. Klaus-Jürgen, Notizen: Hochdrucksynthese und Einkristall-Strukturverfeinerung von Calciumaurat(III), CaAu_2O_4 /High pressure synthesis and single-crystal structure refinement of calcium aurate (III), CaAu_2O_4 , *Z. Naturforsch. B* **51**, 747 (1996).
- [24] J. Park and J. Parise, High-pressure synthesis and structure of a new aurate, CaAu_2O_4 , *Chem. Mater.* **7**, 1055 (1995).
- [25] G. Krämer and M. Jansen, MAu_2O_4 ($M = \text{Sr}, \text{Ba}$), die ersten Oxoaurate(III) mit dreidimensional vernetzter anionischer Teilstruktur, *J. Solid State Chem.* **118**, 247 (1995).
- [26] J. Weinreich and H. Müller-Buschbaum, Zur Kenntnis von $\text{Sr}_5\text{Au}_2\text{O}_8$, *J. Alloys Compd.* **186**, 105 (1992).
- [27] J. Weinreich and H. Müller-Buschbaum, Zur Kenntnis von $\text{Ba}_9\text{Au}_2\text{O}_{12}$, *J. Alloys Compd.* **184**, 187 (1992).
- [28] P. Jiang, S. Porsgaard, F. Borondics, M. Köber, A. Caballero, H. Bluhm, F. Besenbacher, and M. Salmeron, Room-temperature reaction of oxygen with gold: An in situ ambient-pressure X-ray photoelectron spectroscopy investigation, *J. Am. Chem. Soc.* **132**, 2858 (2010).
- [29] J. Kurzman, X. G. Ouyang, W. Im, J. Li, J. Hu, S. Scott, and R. Seshadri, $\text{La}_4\text{LiAuO}_8$ and $\text{La}_2\text{BaPdO}_5$: Comparing two highly stable d^8 square-planar oxides, *Inorg. Chem.* **49**, 4670 (2010).
- [30] K. Kepp, A quantitative scale of oxophilicity and thiophilicity, *Inorg. Chem.* **55**, 9461 (2016).
- [31] M. Higo, Y. Matsubara, Y. Kobayashi, M. Mitsushio, T. Yoshidome, and S. Nakatake, Formation and decomposition of gold oxides prepared by an oxygen-dc glow discharge from gold films and studied by X-ray photoelectron spectroscopy, *Thin Solid Films* **699**, 137870 (2020).
- [32] X. Wang, C. Evans, and D. Natelson, Photothermoelectric detection of gold oxide nonthermal decomposition, *Nano Lett.* **18**, 6557 (2018).
- [33] M. Peuckert, XPS study on surface and bulk palladium oxide, its thermal stability, and a comparison with other noble metal oxides, *J. Phys. Chem.* **89**, 2481 (1985).
- [34] J. Kurzman, L. Misch, and R. Seshadri, Chemistry of precious metal oxides relevant to heterogeneous catalysis, *Dalton Trans.* **42**, 14653 (2013).
- [35] S. J. Ashcroft and E. Schwarzmann, Standard enthalpy of formation of crystalline gold(III) oxide, *J. Chem. Soc. Faraday Trans.* **68**, 1360 (1972).
- [36] Y. Krockenberger, A. Ikeda, K. Kumakura, and H. Yamamoto, Infinite-layer phase formation in the $\text{Ca}_{1-x}\text{Sr}_x\text{CuO}_2$ system by reactive molecular beam epitaxy, *J. Appl. Phys.* **124**, 073905 (2018).
- [37] L. Maya, M. Paranthaman, T. Thundat, and M. L. Bauer, Gold oxide as precursor to gold/silica nanocomposites, *J. Vac. Sci. Technol. B* **14**, 15 (1996).
- [38] A. Klumb, C. Aita, and N. Tran, Sputter deposition of gold in rare-gas (Ar, Ne)- O_2 discharges, *J. Vac. Sci. Technol. A* **7**, 1697 (1989).
- [39] K. Cook and G. Ferguson, Relative lability of gold-oxide thin films in contact with air, solvents, or electrolyte solutions, *J. Vac. Sci. Technol. A* **31**, 021508 (2013).
- [40] M. Horio, Y. Krockenberger, K. Koshiishi, S. Nakata, K. Hagiwara, M. Kobayashi, K. Horiba, H. Kumigashira, H. Irie,

- H. Yamamoto, and A. Fujimori, Angle-resolved photoemission spectroscopy of the low-energy electronic structure of superconducting Pr₂CuO₄ driven by oxygen nonstoichiometry, *Phys. Rev. B* **98**, 020505(R) (2018).
- [41] Y. Seto, RECIPRO, <https://github.com/seto77/Recipro/releases>, v. 4.809.
- [42] S. Preiß, C. Förster, S. Otto, M. Bauer, P. Müller, D. Hinderberger, H. Hashemi Haeri, L. Carella, and K. Heinze, Structure and reactivity of a mononuclear gold(II) complex, *Nat. Chem.* **9**, 1249 (2017).
- [43] A. Jezierski and J. Kaczkowski, Ab-initio study of electronic structure and thermodynamic properties of aurates BaAu₂O₄ and SrAu₂O₄, *Solid State Commun.* **229**, 10 (2016).
- [44] Y. Krockenberger, A. Ikeda, and H. Yamamoto, Atomic stripe formation in infinite-layer cuprates, *ACS Omega* **6**, 21884 (2021).